Numerical Analysis of Elliptical Flange Hole Forming Process

Shasha Dou 1,2

1 College of Mechanical Engineering, Yancheng Institute of Technology, Yancheng, 224051, Jiangsu, China
2 College of Mechanical and Electrical Engineering, Nanjing University of Aeronautics & Astronautics, Nanjing, 211106, Jiangsu, China

Jiansheng Xia*

College of Mechanical Engineering, Yancheng Institute of Technology, Yancheng, 224051, Jiangsu, China
** Corresponding author Email: xiajiansheng@163.com*

Abstract
Under the assumption of Prandtl-Reuss flow rule and von Mises yield criterion, the incremental elasto-plastic large deformation finite element model was established based on the Updated Lagrangian Formulation (ULF).The elasto-plastic conversions of boundary and deformation are reduced with rule. The friction phenomenon of slippage and viscosity at the boundary interface is revised with increment of revision Coulomb rule. The increment rules are led into the whole stiffness matrix, and derived out the stiffness equation. The study shows that the influences on steel elliptical hole flange forming deformation such us punch load, punch stroke thickness, and flanging height were influenced by punch structure and parameter. The dates show that the finite element simulation and experimental results have a good consistency.
Key words: ELASTOPLASTICITY, FEM SIMULATION, ELLIPTICAL HOLE FLANGE.

1. Introduction

Sheet metal forming is a common material processing method, which can be divided into stretching, bending, drawing and flanging, etc. [1]. Its parts can be used in automotive, stationery manufacturing, household appliances industry when provided with the support group or for pipeline connection and other purposes.

The manufacturing process is using the elliptical punch to stretch forming the sheet, and the blank will bend along the punch radius to form an elliptical shape hole. The hole expands with the dropping of the punch, and the thickness near the hole will gradually be thinner. It results the neck and cracked phenomenon. Therefore, the finite element was used to analysis the flange forming process, instead of the trial and error method which were used in general mold factory. This will reduce the costs and shorten development time away [2].

Tang [3] studied the different punches to analyse the distribution of stress and strain in the flange forming with the shell theory and ignoring the bending ef-

fect. Huang and Chien [4, 5] investigated the flange hole shape with the different punch radius and shapes. The results show there is a linear relationship between the initial diameter and after stretching. Takuda and Hatta [6, 7] used the rigid-plastic finite element to simulate the sheet metal forming and used ductile fracture criterion to predict zirconium sheet stretch forming limit. The results show that the extension of zirconium sheet is high, but the stretch is low. Leu [8] studied the numerical analysis and experiment of flange process with the incremental elastic-plastic finite element method. The results can effectively predict the forming process: when hardening index and orthogonal anisotropy increased, the maximum hole expansion ratio also increased. Huang and Chien [9] studied the forming process of the flange hole with the frusto-conical punches and different radius, and found the frusto-conical taper punch radius does not affect the forming, the maximum load decreases with the punch radius increasing.

In this paper, the steel sheet SPCC is analyzed with the finite element method, some relationships are studied, such us: relationship between punch load and displacement, distribution of stress and strain, distribution of thickness. The simulation data is verified by actual experiments which are used to reference for operation and alter design process.

2 Fundamental theory

2.1 Virtual work principle

It descripts the elastic-plastic deformation with the updated Lagrangian formulation ULF [6], the Virtual work principle formulation can be shown as follows:

$$\int_{V^E}\left(\ddot{\sigma}_{ij}-e\sigma_{ik}\dot{\varepsilon}_{kj}\right)\delta\dot{\varepsilon}_{ij}dV+\int_{V^E}\sigma_{jk}L_{ik}\delta L_{ij}dV=\int_{S_f}\dot{f}\delta v_i dS \quad (1)$$

where, $\ddot{}_{ij}$ is the Cauchy stress tensor, $\dot{\varepsilon}_{kj}$ is the rate of stress tensor, $\dot{\varepsilon}_{ij}$ is the strain tensor, σ_{jk} is the rate of strain tensor, $\delta\dot{\varepsilon}_{ij}$ is the virtual strain tensor of the point, δL_{ij} is the virtual velocity gradient tensor of the point, δv_i is the velocity component, $\dot{f}$ is surface force component, L_{ij} is velocity gradient tensor , V is unit volume, S is unit surface area.

2.2 Constitutive relation

In preparing the theory of elasto-plasticity, we have made certain assumptions [10].

(1)The material is homogeneous and isotropic;

(2)There is no strain before manufacturing;

(3)Temperature effect don't consider when manufacturing;

(4)It obeys the laws of the Hooke's Law in elastic stage;

(5)It obeys the von Mises yield rule and Prandtl-Reuss plastic flow rule;

(6)It contains Isotropic strain hardening in constitutive equation;

(7)There are elastic strain stage and plastic strain stage in material strain rate;

(8)Punch, die and holder are steel structure;

(9)The Bauschinger effect don't consider in reverse unloading.

After assuming above, the constitutive relation can be written as follow:

$$\overset{\circ}{\sigma}_{ij}=C^{ep}_{ijmn}\dot{\varepsilon}_{mn} \quad (2)$$

$$C^{ep}_{ijmn}=C^{e}_{ijmn}-\frac{C^{e}_{ijkl}C^{e}_{uv}\dfrac{\partial f}{\partial\sigma_{kl}}\dfrac{\partial f}{\partial\sigma_{uv}}}{C^{e}_{kluv}\dfrac{\partial f}{\partial\sigma_{kl}}\dfrac{\partial f}{\partial\sigma_{uv}}+H'\dfrac{\sigma_{uv}\dfrac{\partial f}{\partial\sigma_{uv}}}{\bar{\sigma}}} \quad (3)$$

where: $\overset{\circ}{\sigma}_{ij}$ is Jaumann differential of σ_{ij}, C^{ep}_{ijmn} is the elastic-plastic module, C^{e}_{ijmn} is Elastic module, f is the initial yield function, H' is the strain hardening rate, $\bar{\sigma}$ is Von Mises yield function, so the Matrix form of C^{ep}_{ijmn} can be expressed as bellow:

$$\left[C^{ep}\right]=\left[C^{e}\right]-\frac{1}{S}\begin{bmatrix} S_1^2 & S_1S_2 & S_1S_3 & S_1S_4 & S_1S_5 & S_1S_6 \\ & S_2^2 & S_2S_3 & S_2S_4 & S_2S_5 & S_2S_6 \\ & & S_3^2 & S_3S_4 & S_3S_5 & S_3S_6 \\ & & & S_4^2 & S_4S_5 & S_4S_5 \\ & & & & S_5^2 & S_5S_6 \\ symm & & & & & S_6^2 \end{bmatrix} \quad (4)$$

Where,

$$S=\frac{4}{9}\bar{\sigma}^2H'+S_1\sigma'_{xx}+S_2\sigma'_{yy}+S_3\sigma'_{zz}+2S_4\sigma'_{yz}+2S_5\sigma'_{zx}+2S_6\sigma'_{xy} \quad (5)$$

$$S_1=2G\sigma'_{xx} \quad S_2=2G\sigma'_{yy} \quad S_3=2G\sigma'_{zz} \quad (6)$$

$$S_4=2G\sigma'_{yz} \quad S_5=2G\sigma'_{zx} \quad S_6=2G\sigma'_{xy} \quad (7)$$

where σ'_{ij} is deviator of σ_{ij}, is the friction flow potential, $G=\sigma_1^2+\sigma_2^2$, $\left[C^e\right]$ is the formula in minimum strain, which can be expressed as bellow:

$$\left[C^{e}\right]=\frac{E}{1+\nu}\begin{bmatrix} \frac{1-\nu}{1-2\nu} & \frac{1-\nu}{1-2\nu} & \frac{1-\nu}{1-2\nu} & 0 & 0 & 0 \\ & \frac{1-\nu}{1-2\nu} & \frac{1-\nu}{1-2\nu} & 0 & 0 & 0 \\ & & \frac{1-\nu}{1-2\nu} & 0 & 0 & 0 \\ & & & \frac{1}{2} & 0 & 0 \\ & & & & \frac{1}{2} & 0 \\ symm & & & & & \frac{1}{2} \end{bmatrix} \quad (8)$$

Where, E is modulus of elasticity, ν is Poisson's ratio. If the material is homogeneous and isotropic,

the Elasto-plastic rate equation can be written:

$$\overset{\circ}{\sigma}_{ij} = \frac{E}{1+\nu}\left[\delta_{ik}\delta_{jl} + \frac{\nu}{1-2\nu}\delta_{ij}\delta_{kl} - \frac{3\alpha\left(\frac{E}{1+\nu}\right)\sigma'_{ij}\sigma'_{kl}}{2\bar{\sigma}^2\left(\frac{2}{3}H' + \frac{E}{1+\nu}\right)}\right]\dot{\varepsilon}_{kl} \tag{9}$$

When α =1, it is a plastic stage; when α =0, it is an elastic stage or unloading stage.

Equivalent stress and equivalent plast C ic strain relations can express by n-power law formulation:

$$\dot{\sigma} = C\left(\varepsilon_0 + \dot{\varepsilon}_p\right)^n \tag{10}$$

Where: C is material constant, n is strain hardening index; $\dot{\sigma}$ is the equivalent stress, $\dot{\varepsilon}_p$ is the equivalent plastic strain, ε_0 is the initial strain.

2.3 Finite element formula

Finite element analysis is the method that the structure is divided into many small units called discrete entity. Based on Large deformation stress and stress rate relation, the finite deformation of Update Lagrangian Formulation, material constitution relationship, the velocity distribution of each unit is show bellow:

$$\{v\} = \leq [N]\{\dot{d}\} \tag{11}$$

$$\{\dot{\varepsilon}\} = \leq [B]\{\dot{d}\} \tag{12}$$

$$\{L\} = \leq [M]\{\dot{d}\} \tag{13}$$

Where, $[n]$ is shape function, $\{d\}$ is nodal velocity, $[B]$ is strain rate-velocity matrix, $[M]$ is velocity gradient-velocity matrix.

The principle of virtual work equation and the constitutive equation based on update Lagrangian is linear equation. The formula can be written by the form of incremental representation.

After finite element discrimination, the large deformation rigid general equation is written as bellow:

$$[K]\{\Delta u\} = \{\Delta F\} \tag{14}$$

Where:

$$[K] = \sum_{\langle E\rangle}\int_{V^e}[B]^T\left([C^{ep}] - [Q]\right)[B]dV + \sum_{\langle E\rangle}\int_{V^e}[E]^T[Z][E]dV \tag{15}$$

$$\{\Delta F\} = \sum_{\langle E\rangle}\int_{S^E}[N]^T\{\dot{f}\}dS\Delta t \tag{16}$$

$[K]$ is the overall Elasto-plastic stiffness matrix, $\{\Delta F\}$ is the nodal displacement increment, $\{\Delta u\}$ is the nodal forces incremental, $[Q]$ and $[Z]$ are stress correction matrix.

$$Q = \begin{bmatrix} 2\sigma_{xx} & 0 & 0 & \sigma_{xy} & 0 & \sigma_{xz} \\ & 2\sigma_{yy} & 0 & \sigma_{xy} & \sigma_{zy} & 0 \\ & & 2\sigma_{zz} & 0 & \sigma_{zy} & \sigma_{xz} \\ & & & \frac{1}{2}(\sigma_{xx}+\sigma_{yy}) & \frac{1}{2}(\sigma_{zx}) & \frac{1}{2}(\sigma_{zy}) \\ & & & & \frac{1}{2}(\sigma_{yy}+\sigma_{zz}) & \frac{1}{2}(\sigma_{xy}) \\ symm & & & & & \frac{1}{2}(\sigma_{xx}+\sigma_{zz}) \end{bmatrix} \tag{17}$$

$$Z = \begin{bmatrix} \sigma_{xx} & 0 & 0 & \sigma_{xy} & \sigma_{xz} & 0 & 0 & 0 & 0 \\ & \sigma_{yy} & 0 & 0 & 0 & \sigma_{xy} & \sigma_{yz} & 0 & 0 \\ & & \sigma_{zz} & 0 & 0 & 0 & 0 & \sigma_{xz} & \sigma_{yz} \\ & & & \sigma_{yy} & \sigma_{yz} & 0 & 0 & 0 & 0 \\ & & & & \sigma_{zz} & 0 & 0 & 0 & 0 \\ & & & & & \sigma_{xx} & \sigma_{xz} & 0 & 0 \\ & & & & & & \sigma_{zz} & 0 & 0 \\ & & & & & & & \sigma_{xx} & \sigma_{xy} \\ symm & & & & & & & & \sigma_{yy} \end{bmatrix} \tag{18}$$

2.4 Friction processing

There is friction in sheet forming process, so we need to pay attention to materials and tools of the interface conditions [11]. When the material moves along the tool surface curve of the slide, the contact force can be expressed as:

$$F = F_l l + F_n n \tag{19}$$

Where, F_l is radial force and F_n is normal force, and differential equation of F can be expressed as:

$$\dot{F} = \dot{F}_l l + F_l \dot{l} + \dot{F}_n n + F_n \dot{n} \tag{20}$$

Where, differentials of $\dot{l}$ and $\dot{n}$ are expressed as:

$$\dot{l} = -\Delta u_l^{rel} / R \tag{21}$$

$$\dot{n} = \Delta u_l^{rel} / R \tag{22}$$

Where, R is tool radius, Δu_l^{rel} is the local relative velocity between the tool and node, and the nodes relative speed can be expressed as:

$$\Delta u_l^{rel} = \Delta u_l - \dot{u}_{tool}\sin\theta \tag{23}$$

Where, Δu_l is the contact tangent displacement increment of nodes, $\dot{u}_{tool}$ is the displacement increment of tooling, θ is the rotation angle.

The increment formula of $\dot{F}$ is expressed as follow:

$$\dot{F} = \left(\dot{F}_l - F_n\Delta u_l / R + F_n\dot{u}_{tool}\sin\theta / R\right)\cdot l + \left(\dot{F}_n - F_l\Delta u_l / R - F_l\dot{u}_{tool}\sin\theta / R\right)\cdot n \tag{24}$$

Rigid matrix governing equation of the contact nodes is expressed bellow:

$$\begin{bmatrix} K & \cdots & \cdots \\ \cdots & K_{11} + F_n / R & K_{12} \\ \cdots & K_{21} + F_n / R & K_{22} \end{bmatrix}\cdot\begin{Bmatrix} \cdots \\ \Delta u_l \\ \Delta u_n \end{Bmatrix} = \begin{Bmatrix} \cdots \\ \dot{F}_l + F_n\dot{u}_{tool}\sin\theta / R \\ \dot{F}_l - F_l\dot{u}_{tool}\sin\theta / R \end{Bmatrix} \tag{25}$$

2.5 Incremental steps of $r_{\min}$ method

Using the elastic plastic finite element method with large deformation method, also called the Yamada $r_{\min}$ method. Each incremental step value is equal to incremental displacement of initial deformation increment of the tooling. Adopting the method of updated Lagrangian formulation, calculating each increment of displacement, strain, stress, load, springback value after forming the final shape of sheet mental in unloading condition, the value of load incremental in each step is controlled by $r_{\min}$ formula, which is shown as bellow:

$$r_{\min} = MIN(r_1, r_2, r_3, r_4, r_5) \quad (26)$$

Where, r_1 is The maximum allowable strain increment, r_2 is the maximum allowable rotation increment, r_3 is the minimum value in all elastic elements, r_4 is contact position between free node and tooling, r_5 is discontent position between free node and tooling.

3 Numerical analysis flow

Based on the finite deformation theory, ULF equation and method, a set of effective analysis of sheet metal forming process is established. Firstly, a 3d part and mold was designed with the NX software, and then meshed themith NASTRAN software. Secondly, the meshed models were drawn into the data file and with finite element analysis. The simulation flow chart is shown in Figure 1.

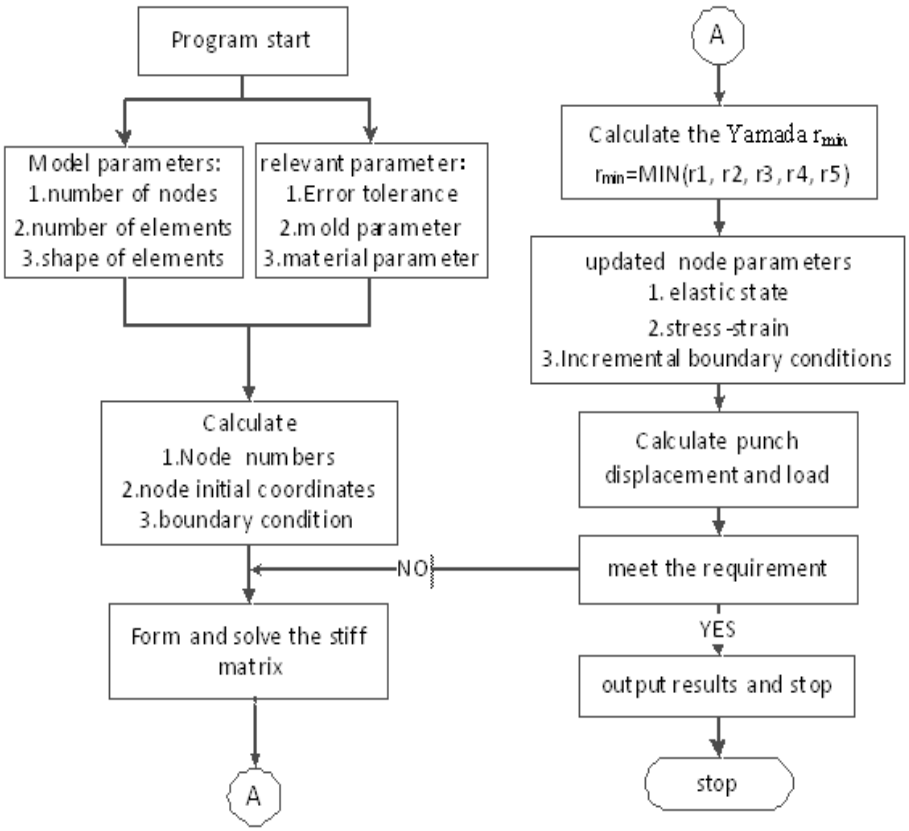

Figure 1. Numerical simulation of flow chart

Based on the theory upwards, the research of steel elliptical cup drawing is studied, including relationship between the punch load and displacements, stress and strain, thickness, spring-back and warpage. Simulation experimental parameters were carried out, which are friction coefficient (μ), punch radius (r_p), die radius (R_d). The parameters of warpage problems are verified by the experiment are optimized and served a reference for drawing designer.

The whole structure is composed of punch, die and blank holder. The model picture was shown as Figure 2.

As shown in Figure 2, it takes two coordinates to solve the problem, which are fixed coordinates (X, Y, Z) and local coordinates (ξ, η, ζ). It uses the fixed coordinates (X, Y, Z) when nodes do not contact with the tool, and uses the local coordinates (ξ, η, ζ) when nodes contact with the tooling. Using coordinates rule based on the right-hand rule.

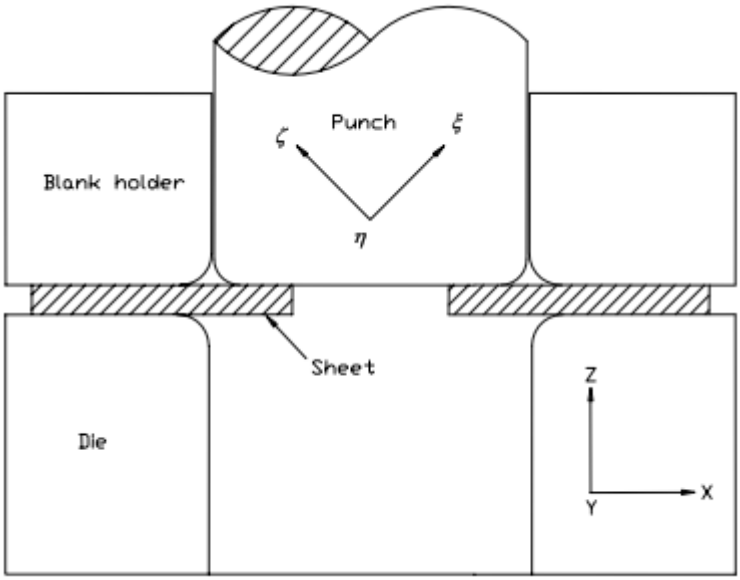

Figure 2. Sheet metal and die size chart

The contact condition of each node of plates will change depending on deformation in sheet metal forming. When the displacement increment is zero, the boundary conditions of increment displacement of the next node will changes to free node boundary conditions. When sheet contacts the tools, contact condition is changed to the boundary conditions, which bases on the generalized $r_{\min}$ method.

Blanks preparation: JIS SPCC steel sheet, cutting into the outer diameter 130mm and an initial elliptical hole in the center of the sheet by CNC, the long axis of elliptical size 23mm, short axis dimension 12mm.

Experimental arrangement: the sheet metals were put on hydro forming machine, the the sheet center was consistent with the mold. The pressure was 160kN, and the punch speed was 1.0mm/s. The simulation datas of punch load and the punch stroke were measured. Finally, Experimental datas of the flange heights were measured and recorded with calipers.

JIS SPCC material stainless steels were provided by a china steel Crop, of which the mechanical properties as shown in Table 1 [12].

Table 1. Mechanical properties of JIS SPCC

stress-strain relationship: $\bar{\sigma}=563.64(0.011+\bar{\tau}_p)^{0.2781}$			
initial thickness	t =0.6mm	Poisson's ratio	ν =0.3
yield stress	σ_y =163.5MPa	Anisotropy value	r_0 =1.71, r_{45} =1.52, r_{90} =2.11
Yang coefficient:	E =2.1×105 MPa		

Because of the symmetrical sheet model, 1/4 model was taken to analysis.

The quadrilateral segmentation of degenerated shell element was used in sheet metal meshing, and the triangle segmentation was used in the die meshing.

4 Results

4.1 Punch load analysis

Simulation experiments were carried out with different friction coefficients (μ =0.1 and μ =0.2), which were compared with the experimental data. The relationship between the punch load and storke was shown in Figure 3. As can be seen from the figure, the punch load increases gradually with the punch stroke. When the punch stroke is 8.0mm, the maximum load value is 4890N. The sheet continues deformation with the increasing of the punch displacement. Because of circumferential tensile stress, the flanging hole continues to expand and thiner, and the load leveles off until the punch through the die.

4.2 Flange height analysis

The changing height of the hole flange was shown as Figure 4. Measuring points located from the long-axis to short axis which was from 0 to 90 degrees. The initial hole circumference was 28.20mm. The hole perimeter increased to 39.40mm and elongation rate was 39.68% with the effect of tensile deformation. The flange height position was lowest, and increased along the direction of the short axis.

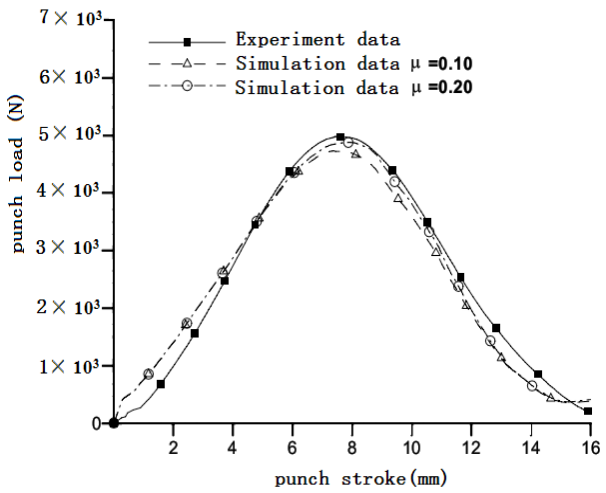

Figure 3. The relationship between the punch load and stroke

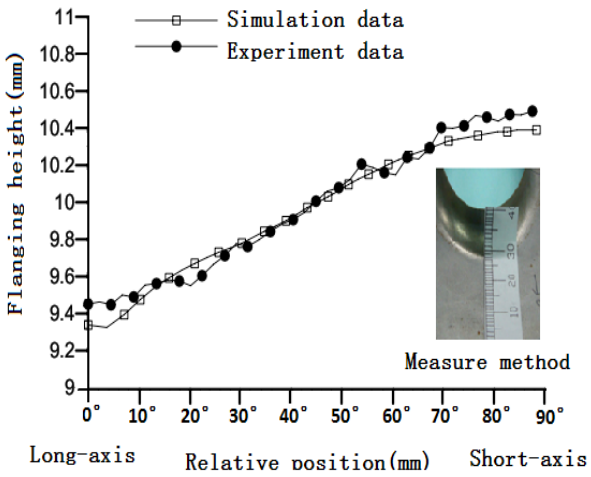

Figure 4. Thickness change analysis in long axis and short axis

4.3 Different punch radius and initial hole diameter limit analysis

In order to find out changes rules of punch load and punch stroke, some experiments were carried out with the different punch fillet radius, which were R =3.0mm, R =5.0mm, R =7.0mm, R =9.0mm and R =11.0mm. Experiments with four different dimension of initial elliptical hole were carried out. The different elliptical hole dimension were a =23mm b =12mm, a =22mm b =11mm, a =21mm, b =10mm, a =20mm and b =9mm.

The relationship between the maximum punch load and diameters with different elliptical holes dimension were shown as Figure 5. It can be seen from the figure, the maximum punch load significantly increases when the initial elliptical hole dimension and the radius of punch fillet decreases.

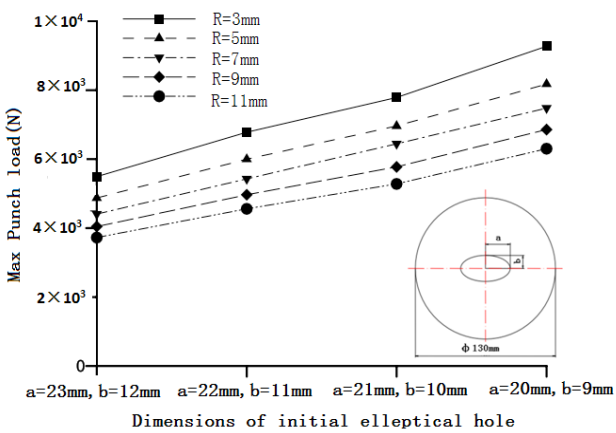

Figure 5. The punch load distribution with different elliptical holes and punch fillets

The relationship between the maximum punch stroke and diameters with different elliptical holes dimension was shown as Figure 6. It can be seen from the figure shows that maximum punch stroke significantly increases when the initial dimension of elliptical holes decreases and the punch fillet radius increases.

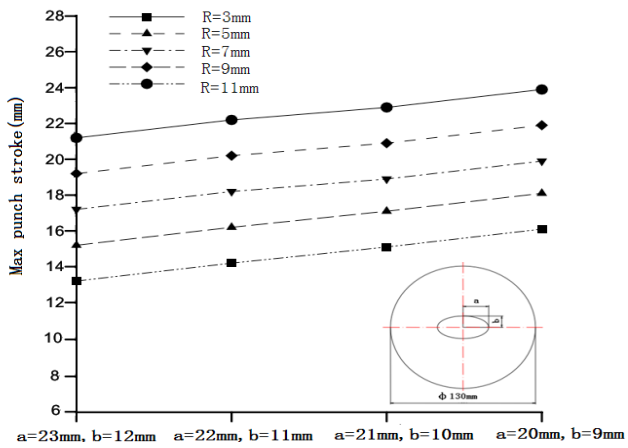

Figure 6. The punch stroke distribution with different elliptical holes and punch fillets

4.4 Thickness analysis with different axial ratio

The simulation of the punch load, thickness and flanging height with different axial ratio (a/b) were carried out.

The punch load distributions with different axial ratio (a/b) was shown as Figure 7. It shows the same trend curve before the maximum value, the load fells faster with higher axial ratio (a/b) after maximum value.

The thickness of long-axis distribution with different axial ratio (a/b) was shown as Figure 8. It can be seen from the figure, the thickness increases when axial ratio (a/b) decreases, until the smallest thickness which is close to fracture thickness.

The reason is when the axial ratio was larger, the tensile stress in the long axis was the larger, and thickness was thinner. Long axis edge was easy to rupture.

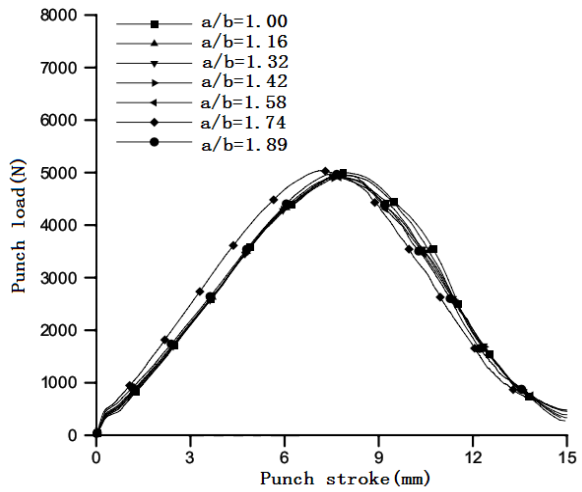

Figure 7. The punch load distribution with different axial ratio

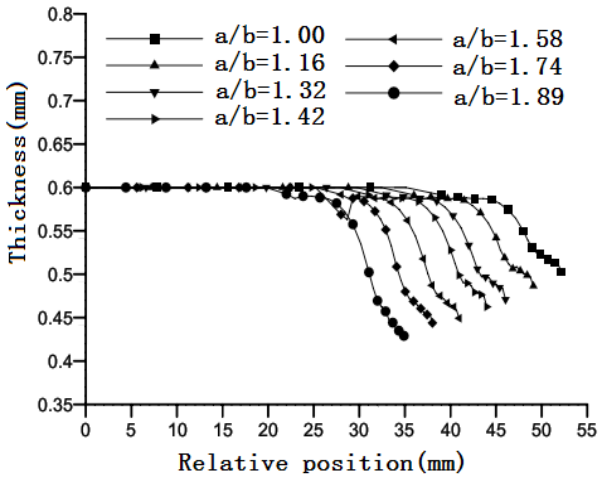

Figure 8. The thickness of long-axis distribution with different axial ratio

The short-axis thickness distribution with different axial ratio (a/b) was shown as Figure 9. It can be seen from the figure, the thickness increases when axial ratio (a/b) increases, the smallest value was near the short axis edge.

The circumference thickness distribution with different axial ratio (a/b) was shown as Figure 10. It can be seen from the figure, the thickness decreases in relative position 0-10mm when axial ratio (a/b) increases, and the thickness increases in relative position more than 10mm when axial ratio (a/b) increases.

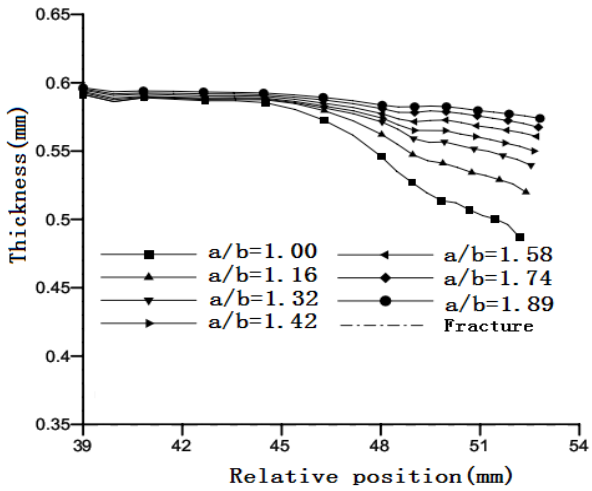

Figure 9. The thickness of short-axis distribution with different axial ratio

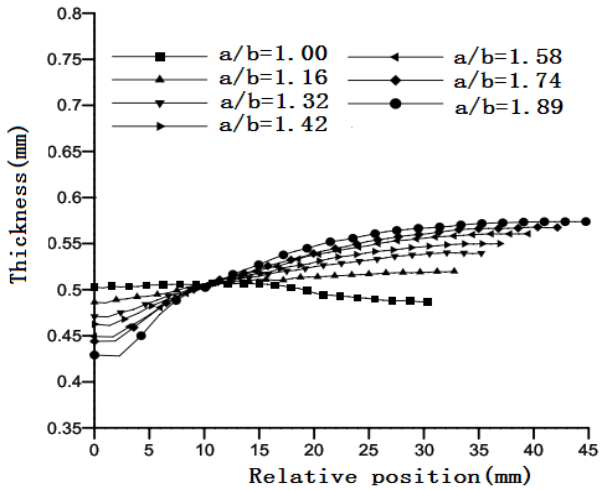

Figure 10. The thickness along the elliptical hole distribution with different axial ratio

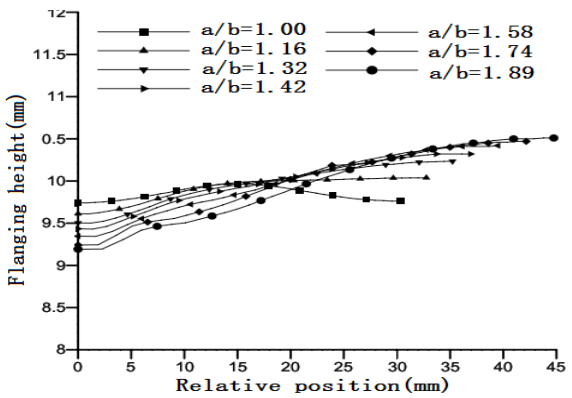

Figure 11. The flanging height distribution with different axial ratio

The flanging height distribution with different axial ratio (a/b) are shown as Figure 11. It can be seen from the figure, the height decreases in relative position 0-20mm when axial ratio (a/b) increases, and the thickness increases in relative position more than 20mm when axial ratio (a/b) increases.

5. Conclusions

With the advancement in networking and multimedia technologies enables the distribution and sharing of multimedia content widely. In the meantime, piracy becomes increasingly rampant as the customers can easily duplicate and redistribute the received multimedia content to a large audience.

Based on the numerical analysis and experimental results, combined with finite element method and the incremental Elasto-plastic theory, those were analyzed which include stress distribution, thickness, forming limit and punch radius. It obtains the following conclusions.

(1) The punch load increases gradually with the punch stroke. When the punch stroke is 8.0mm, the maximum load value is 4890N.

(2) The maximum punch stroke significantly increases with the initial dimension decreasing of elliptical holes and increasing of the punch fillet radius.

(3) In the long-axis, maximum punch load decreases with the increasing of punch radius and initial elliptical hole diameter.

(4) The punch load increases with the decreasing of initial elliptical hole dimension and the radius of punch fillet.

(5) The long-axis thickness increases when axial ratio (a/b) decreases, until closing to fracture thickness. The short-axis thickness increases when axial ratio (a/b) increases, the smallest value occurs near the short axis edge.

(6) The thickness and flanging height firstly decreases with axial ratio (a/b) increasing, and then decreases with axial ratio (a/b) increasing.

Acknowledgements

This work was supported by The National Natural Science Foundation of China (Grant No. 51505408). The Natural Science Foundation for General Universities of Jiangsu Province, China (No.12KJD520010). The National Spark Program Project, China (No. 2014GA690214). Jiangsu Intelligent Mould Manufacturing Engineering Technology Research Center.

References

1. JS Xia; SS Dou (2013) Experimental Research on the Flanging Height Adjustment Based on Environmental Way International. *Journal of Applied Environmental Sciences*, 8(20), p.p. 2470-2489.
2. JS Xia, SS Dou (2014) The study on steel elliptical cup drawing based on finite element analysis. *Computer Modelling and New Technologies,* 18(10), p.p. 7-13.
3. JS Xia, SS Dou. (2014) Numerical analysis of sheet metal U-Bending process. *Computer Modelling and New Technologies,* 18(11), p.p.159-165.
4. T. Kumagai, H. Saiki and Y. Meng (1999) Hole Flanging with Ironing of Two-Ply Thick Sheet Metals. *Journal of Materials Processing Technology*, 8 (9), p.p.51-57.
5. Y. M. Huang and K. H. Chien (2001) The Formability Limitation of the Hole-Flanging Process. *Journal of Materials Processing Technology*, 117(1), p.p. 43-51.
6. Y. M. Huang and K. H. Chien (2001) Influence of the Punch Profile on the Limitation of Formability in Hole-Flanging Process. *Journal of Materials Processing Technology*, 113(1), p.p. 720-724.
7. H. Takuda and N. Hatta (1998) Numerical Analysis of Formability of a Commercially Pure Zirconium Sheet in Some Forming Processes. *Materials Science and Engineering*, 242(1), p.p. 15-21.
8. D. K. Leu (1996) Finite-Element Simulation of Hole-Flanging Process of Circular Sheets of Anisotropic Materials International. *Journal of Mechanical Sciences*, 38(8), p.p. 917-933.
9. Y. M. Huang and K. H. Chien (2002) Influence of Cone Semi-Angle on theFormability Limitation of the Hole-Flanging Process International. *Journal of Advanced Manufacturing Technology*, 19(8), p.p. 597-606.
10. L. C. Sousa, C. F. Castro and C. A. C. Antonio (2006) Optimal Design of V and U Bending Processes Using Genetic Algorithms. *Journal of Material Processing Technology*, 172, p.p. 35-41.
11. G. Liu, Z. Lin, W. Xu and Y. Bao (2002) Variable Blankholder Force in U-Shaped Part Forming for Elimination Springback Error. *Journal of Material Processing Technology*, 120, p.p. 259-264.
12. Samuel M. (2012) Experimental and numerical prediction of springback and side wall curl in u-bending of anisotropic sheet metals. *Journal of Materials Processing Technology*, 3(105), p.p.382-393.